



OPEN Mathematical modeling of sorption isotherms and the thermodynamic properties of vacuum-dried and freeze-dried Barhi dates

Mohamed Fikry^{1,2}, Saleh Al-Ghamdi³, Bandar Alfaifi³, Mansour N. Ibrahim³, Nashi Alqahtani^{4,5}, Muhammad Umar¹ & Kitipong Assatarakul¹✉

Studying the moisture sorption behavior of Barhi dates is key to enhancing their drying efficiency, packaging strategies, and storage conditions to ensure long-term stability and shelf-life. This research analyzed the sorption isotherms of vacuum-dried (VDBD) and freeze-dried Barhi dates (FDBD) via a dynamic vapor sorption apparatus across different temperatures and a wide range of water activity levels. Various mathematical models were evaluated to determine their accuracy in predicting sorption behavior, and the thermodynamic properties of sorption were examined in relation to the equilibrium moisture content (X_e). The results demonstrated that VDBD and FDBD followed Type III adsorption and Type V desorption isotherms. Adsorption increased with increasing water activity, whereas desorption displayed the opposite trend, with significant hysteresis between the two processes. The Peleg model provided a precise fit for both the adsorption and desorption isotherms across all the tested conditions. To maintain safe storage at the studied temperatures and 50% relative humidity, the recommended moisture content was 5% for VDBD and 9% for FDBD. Additionally, the net isosteric heat of sorption (Q_{st}), differential entropy (ΔS), and Gibbs free energy (ΔG) exhibited inverse correlations with X_e , increasing as the moisture content decreased during sorption. These thermodynamic parameters were effectively modeled as functions of X_e , indicating that both adsorption and desorption were nonspontaneous processes. This study provides critical insights for food processors to refine drying protocols and establish optimal storage conditions for VDBD and FDBD, ultimately preserving quality and preventing microbial contamination.

Keywords Barhi date, Drying, Dynamic vapor sorption isotherms, Mathematical modeling, Thermodynamic properties

The palm date tree is widely cultivated across various regions worldwide, and its fruit is highly consumed for its high nutritional content, including minerals, carbohydrates, fiber, and vitamins. It also possesses anticarcinogenic, antimutagenic, and antioxidant properties that may aid in treating diseases such as cancer, cardiovascular conditions, and stroke^{1,2}. The growing interest in cultivating various palm date varieties is evident in FAO (2023) statistics, which report an annual global production of approximately 10 million tons.

Among the cultivated varieties, Barhi dates are highly valued for their crunchy texture, sweet taste, and bright yellow color at the Khalal (unripe full-colored) stage. This stage has a short marketing window, making it economically significant¹. However, Barhi dates ripen rapidly, transitioning to the Rutab (mature soft brown) stage within approximately seven days postharvest, leading to quality deterioration due to natural biological processes under standard storage conditions^{3,4}.

Maintaining the quality of Barhi dates at the Khalal stage is a major challenge in postharvest management⁵. Improper handling can result in significant losses, both in quality and economic value. To mitigate these losses and prolong shelf-life, researchers have explored various preservation methods, including drying⁶, freeze drying⁷,

¹Department of Food Technology, Faculty of Science, Chulalongkorn University, 10330 Bangkok, Thailand.

²Department of Agricultural and Biosystems Engineering, Faculty of Agriculture, Benha University, Moshtohor, Toukh 13736, Egypt. ³Department of Agricultural Engineering, College of Food and Agriculture Sciences, King Saud University, P.O. Box 2460, Riyadh 11451, Kingdom of Saudi Arabia. ⁴Date Palm Research Center of Excellence, King Faisal University, Al-Ahsa 31982, Saudi Arabia. ⁵Department of Food and Nutrition Sciences, College of Agricultural and Food Sciences, King Faisal University, Al-Ahsa 31982, Saudi Arabia. ✉email: kitipong.A@chula.ac.th

freezing⁸, different packaging materials⁹, and modified atmosphere packaging¹⁰. Therefore, understanding the moisture sorption behavior of Barhi date is crucial for optimizing its drying, packaging, and storage conditions to ensure the stability and extend the shelf-life of Barhi date fruit.

Owing to the influence of water content on the preservation and storage of Barhi date, it is essential to investigate the behavior of moisture sorption isotherms, which describe the correlation between the equilibrium moisture content (X_e) of food material and its corresponding relative humidity (RH) at a constant temperature, covering a range of RH values¹¹. These isotherms offer valuable information about the degree of water binding within a material¹². They are crucial for assessing a material's ability to retain water under particular storage conditions (e.g., temperature and relative humidity).

Several techniques have been utilized for measuring moisture sorption isotherms of various food products, with the gravimetric technique being the most commonly used technique^{13–16}. This method monitors mass alterations, which can be accomplished continuously or intermittently in either dynamic or static systems. Continuous approaches utilize electrobalances to track weight fluctuations, whereas discontinuous methods use salt solutions under either vacuum or atmospheric conditions to determine the equilibrium relative humidity (RH) of the food material¹⁷. Discontinuous systems, however, can face issues such as slow equilibration and the risk of microorganism growth at high RH. These challenges are addressed by the dynamic vapor sorption (DVS) technique. In contrast to saturated salt solutions, a mixture of dry nitrogen and saturated water vapor is utilized in the DVS system to reach the target RH. This approach enables quicker equilibration because of the small sample chamber and continuous nitrogen flow while preventing microorganism growth. As a result, it allows for the measurement of both adsorption and desorption isotherms using the same sample¹⁸.

The examination of moisture sorption isotherms provides valuable thermodynamic insights that are necessary for designing equipment for various preservation processes¹⁹. These properties, including enthalpy, entropy and Gibbs free energy, are crucial for understanding the molecular interactions and processes taking place within food materials²⁰. Additionally, mathematical modeling is essential for defining sorption isotherms and their thermodynamic properties. Various mathematical equations have been developed to describe moisture sorption in food materials, including Peleg²¹, Oswin²², modified Oswin²³, GAB¹², Halsey²⁴, modified Halsey²⁵, BET^{26,27}, modified Henderson²⁸, modified Chung-Pfost²⁹ and Adam and Shove³⁰.

Few studies have been conducted on the moisture sorption of palm date fruit, including those by Mediani, et al.³¹, Moitte and Heikal³², Knani, et al.³³, Ferradji and Matallah³⁴. To the best of the authors' knowledge, no published studies have investigated the moisture sorption of vacuum-dried Barhi dates (VDBD) and freeze-dried Barhi dates (FDBD) at various temperatures or explored their related thermodynamic properties. Hence, this study aimed to explore the adsorption and desorption isotherms of VDBD and FDBD across a broad range of water activity levels at various temperatures, determine the most appropriate model for fitting the sorption isotherms, and evaluate the thermodynamic characteristics related to moisture adsorption and desorption in VDBD and FDBD.

Materials and methods

Sample preparation

Fresh Barhi date fruits and freeze-dried Barhi dates (FDBD) were purchased from a local market in Riyadh, Saudi Arabia, for this study. To prepare vacuum-dried Barhi dates (VDBD), the fresh dates were washed, deseeded, and cut into two halves using a stainless-steel knife. Each fruit was cut, each approximately 2 cm × 2 cm × 1 cm in size to ensure consistent exposure to the experimental conditions. The samples were then dried to a predetermined moisture content via a vacuum oven (LABOCON, Model: LV-103, UK) at 70 °C and a vacuum pressure of 200 mm Hg until a constant weight was achieved. These drying conditions were selected primarily for research purposes, with the goal of achieving a balance between effective moisture removal and the preservation of thermo-sensitive nutrients and structural integrity of the Barhi dates. This temperature falls within the commonly recommended range for drying high-sugar fruits under vacuum conditions. The dried samples were vacuum sealed in polyethylene bags and stored at 5 °C until further analysis of their sorption isotherms. The schematic view of the experimental setup is illustrated in Figure (1).

Determination of moisture content and water activity

The initial moisture content of the samples ($64.3 \pm 1\%$ wet basis, w.b.) was determined following AOAC³⁵ guidelines. Approximately 5 g of date pulp were weighed and placed in a pre-weighed moisture dish, then dried in a laboratory hot air oven at 105 ± 1 °C for 24 h to a constant weight. The initial water activity (0.946 ± 0.003) was determined via a water activity meter (Aqua Lab, Model: Series 3, Decagon Devices Inc., USA). Each sample was analyzed in triplicate, and the mean value was calculated. As a result, VDBD exhibited a moisture content of 5.0 ± 0.2 g/100 g dry basis and a_w of 0.108 ± 0.002 . In comparison, FDBD had a slightly higher moisture content of 9.0 ± 0.3 g/100 g dry basis and an a_w of 0.107 ± 0.003 .

Sorption isotherm analysis via a dynamic vapor sorption (DVS) system

The moisture absorption and release properties of the Barhi dates were examined via a DVS system (Aquadyne DVS, Quantachrome Instruments, Florida, USA). This advanced instrument precisely regulates the relative humidity (RH) and temperature, allowing continuous tracking of sample weight variations. The system consists of several essential components, such as a humidifier, an electronic microbalance, a relative humidity sensor,

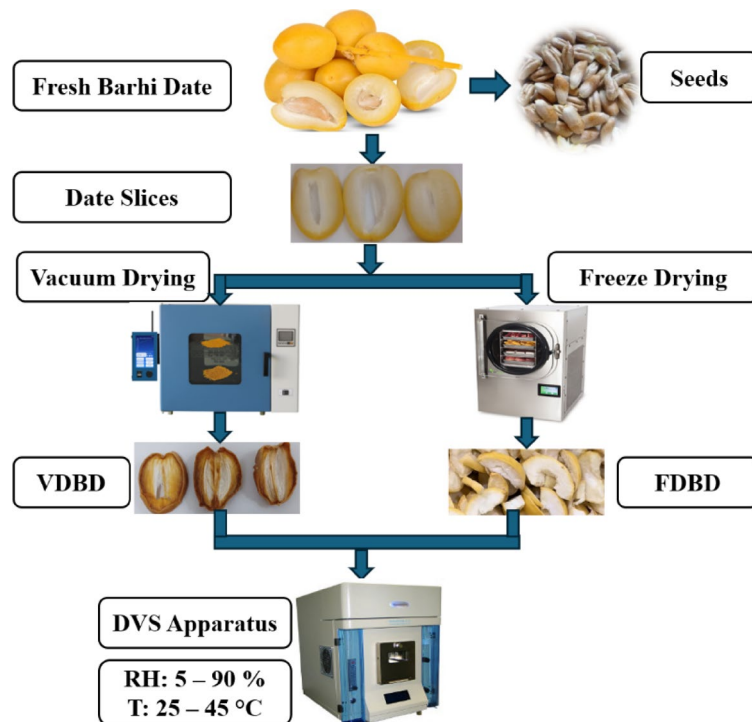


Fig. 1. Schematic view of the experimental setup.

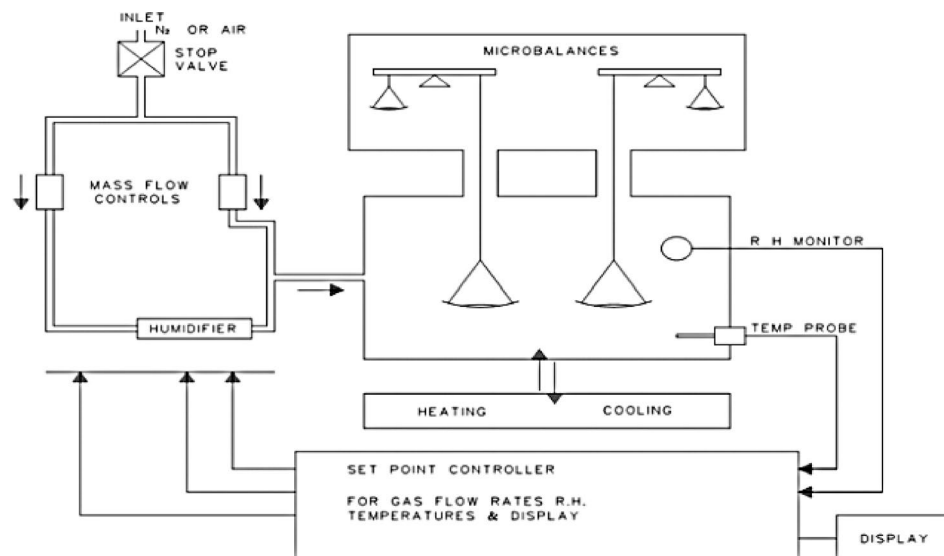


Fig. 2. Systematic diagram of the AQUADYNE DVS.

electronic mass flow controllers, a temperature controller, and a microprocessor linked to a PC. The configuration of the instrument is shown in Fig. 2.

Following the methodology described by Fikry and Al-Awaadh¹¹, predried VDBD and FDBD samples weighing 141.09 ± 0.6 mg were placed inside the analyzer. The experiment was conducted by varying the RH level from 5 to 90% in increments of 10%, ensuring that each step was maintained until equilibrium was achieved, which was defined as a mass fluctuation of less than 0.01% per minute (Fig. 3). Equilibrium conditions were typically reached within approximately 16 and 10 hours for adsorption and desorption phases, respectively. The study was performed at three fixed temperatures (25, 35, and 45 °C) to evaluate how temperature influences moisture sorption. After the adsorption phase was complete, the RH was gradually decreased to investigate the desorption patterns and hysteresis effects. At each humidity level, the equilibrium moisture content (X_e), expressed as the mass of water per unit mass of dry solids, was determined to generate sorption isotherms.

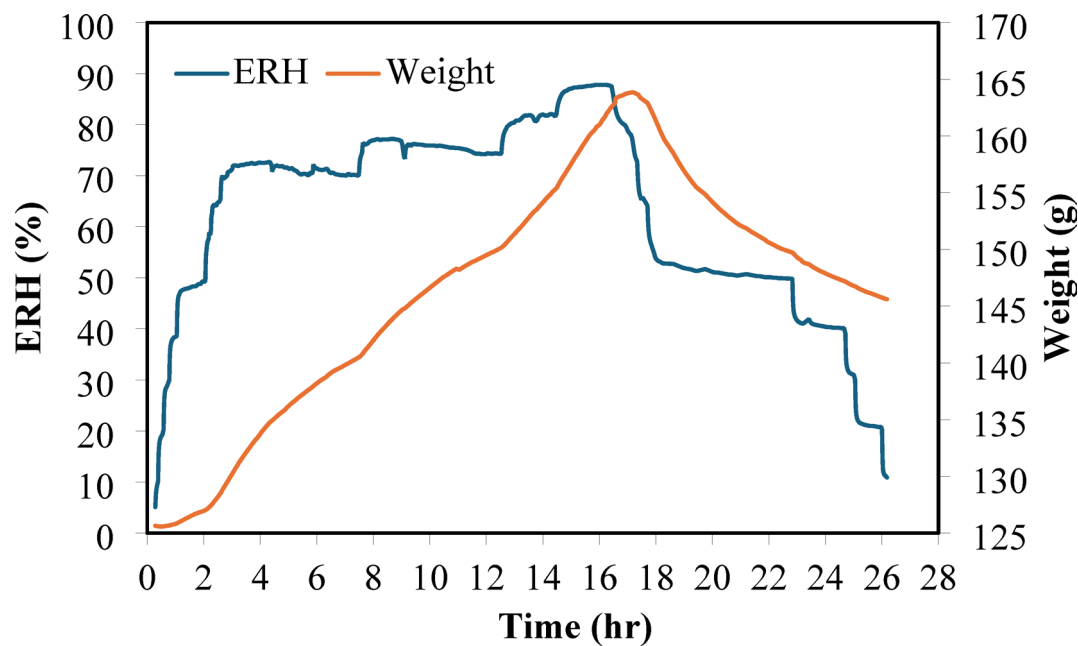


Fig. 3. Time-based representation of moisture sorption for dried Barhi date subjected to gradual shifts in equilibrium relative humidity (ERH) and sample weight at 25 °C.

No	Model name	Equation	References
1	Peleg	$X_e = C_1(a_w)^{C_2} + C_3(a_w)^{C_4}$	Peleg ²¹
2	GAB	$X_e = \frac{X_m C K a_w}{(1 - K a_w)(1 - K a_w + C K a_w)}$	Van den Berg ⁵³
3	BET	$X_e = \frac{X_m C a_w}{(1 - a_w)(1 - a_w + C a_w)}$	Brunauer ²⁶
4	Halsey	$X_e = \left(-\frac{A}{\ln a_w}\right)^{1/B}$	Halsey ²⁴
5	Oswin	$X_e = A(a_w/1 - a_w)^B$	Oswin ²²
6	Smith	$X_e = A - B(\ln(1 - a_w))$	Smith ²⁷
7	Adam and Shove	$X_e = A + B a_w + C a_w^2 + D a_w^3$	Chirife ³⁰

Table 1. Mathematical models applied to the actual sorption isotherm data of VDBD and FDBD. X_e is the equilibrium moisture content (g/g dry solid); X_m is the monolayer moisture content (g/g dry solid); A, B, C, C_1 , C_2 , C_3 , C_4 , D, K, and n are model constants (dimensionless).

Mathematical modeling of sorption isotherm data

Seven commonly utilized mathematical equations—*Peleg*, *GAB*, *BET*, *Halsey*, *Oswin*, *Smith*, and *Adam and Shove*—were applied to analyze the sorption data. Table 1 presents the selected models, which were utilized to assess the experimental adsorption and desorption behavior of VDBD and FDBD.

Evaluation of the thermodynamic characteristics of sorption isotherms

Thermodynamic properties, including the isosteric heat of sorption, differential entropy and Gibbs free energy, serve as key indicators of the complex relationship between food materials and moisture. The heat of sorption reflects the strength of the attraction between the sorption sites and water vapor molecules³⁶. Consequently, understanding the relationship between moisture content and water activity is crucial for characterizing this energy exchange.

The net isosteric heat of sorption (q_{st}), also known as the differential enthalpy of sorption (ΔH), can be determined by analyzing moisture sorption data via Eq. (1). In this study, q_{st} was calculated via the Clausius–Clapeyron equation, as formulated by Lehmad, et al.³⁷ in Eq. (2). Additionally, the isosteric heat of sorption and differential entropy (ΔS) for both water adsorption and desorption at different moisture levels were calculated by applying Eq. (3) to the sorption data. By graphing $\ln(a_w)$ versus $1/T$ at a constant moisture content, q_{st} was computed from the slope, which is represented as $-q_{st}/R$, whereas ΔS was obtained via the linear constant ($\Delta S/R$). This procedure was repeated for various moisture contents to investigate the relationship between q_{st} and moisture content. Notably, this method assumes that the

isosteric heat of sorption is constant through varying temperatures and requires sorption data to be gathered at a minimum of three temperature levels³⁸.

$$q_{st} = Q_{st} - \lambda \quad (1)$$

$$\left[\frac{d \ln(a_w)}{d \left(\frac{1}{T} \right)} \right] = - \frac{q_{st}}{R} \quad (2)$$

$$\ln(a_w) = - \frac{q_{st}}{RT} + \frac{\Delta S}{R} \quad (3)$$

The latent heat of vaporization (λ) of pure water (J/mol) was calculated via Eq. (4), whereas Eq. (5) was used to compute the Gibbs free energy (ΔG).

$$\lambda = R[6687 - 5.31 * T] \quad (4)$$

$$\Delta G = -RT \ln(a_w) \quad (5)$$

where Q_{st} represents the isosteric heat of sorption (J/mole). T corresponds to the absolute temperature (K), and R denotes the universal gas constant (8.314 J/mol.K). Additionally, ΔS refers to the differential entropy (J/mol.K), q_{st} signifies the differential enthalpy or net isosteric sorption heat (J/mol), and ΔG denotes the Gibbs free energy (kJ/mol).

To describe the variation of thermodynamic properties with equilibrium moisture content (X_e), regression models were fitted to the calculated values of net isosteric heat of sorption (Q_{st}), entropy change (ΔS), and Gibbs free energy (ΔG). Non-linear relationships such as cubic, exponential and power equations were applied as it was described previously by Fikry and Al-Awaadh¹¹, Fikry, et al.¹⁴.

Data analysis

To estimate the accuracy of the mathematical models in fitting the actual data obtained from the sorption experiments (Eqs. 6–8), the following statistical metrics were used: the coefficient of determination (R^2), sum of squared errors (SSE) and mean relative percent error (PE%), which was calculated using absolute values to avoid offsetting positive and negative deviations, as shown in Eq. 8. These metrics were calculated via IBM SPSS (v27) software. The model that best fit the data were selected on the basis of specific criteria, including an R^2 value of 0.90 or higher, the lowest SSE and a PE% under 10%, as outlined by Fikry, et al.³⁹.

$$R^2 = 1 - \frac{\sum_{i=1}^N (X_{exp} - X_{pred})^2}{\sum_{i=1}^N (X_{exp} - \bar{X}_{exp})^2} \quad (6)$$

$$SSE = 1/N \sum_{i=1}^N (X_{exp} - X_{pred})^2 \quad (7)$$

$$PE(\%) = \frac{100}{N} \sum_{i=1}^N \frac{|X_{exp} - X_{pred}|}{X_{exp}} \quad (8)$$

In this equation, X_{exp} , X_{pred} , and \bar{X}_{exp} denote the experimental, predicted, and average X_e values (g_w/g_{dm} dry basis, d.b.), respectively. N refers to the total number of experimental data points.

Results and discussion

Mathematical modeling of sorption isotherms

Mathematical modeling of sorption isotherms is essential for predicting moisture behavior in foods, optimizing drying and storage conditions, and ensuring product stability and quality. This study utilized seven equations—Peleg, GAB, BET, Halsey, Oswin, Smith, and Adam and Shove—to characterize sorption isotherms and moisture dynamics in the VDBD and FDBD. The determined constants of the models applied to the sorption data of VDBD and FDBD at various temperatures are shown in Tables 2 and 3, respectively. The optimal model was selected on the basis of the following criteria: achieving the highest correlation coefficient ($R^2 \geq 0.90$), the lowest percentage error (PE%) (below 10%), and the minimum sum of squared errors (SSE) values (close to zero), as emphasized by Fikry, et al.³⁹. The statistical fitting parameters of the models applied to the sorption data of VDBD and FDBD at various temperatures are shown in Tables 4 and 5, respectively.

Upon comparison, the Peleg model consistently demonstrates the best performance for both VDBD and FDBD across various parameters. The average SSE values for adsorption and desorption are notably low, with VDBD adsorption having an average SSE of 1.87×10^{-4} and desorption at 1.67×10^{-3} . For FDBD, the average SSE for adsorption is 5.66×10^{-4} and desorption is 4.22×10^{-5} . In terms of R^2 , the Peleg model provides near-perfect fits at all temperatures, with VDBD averaging 0.996 for adsorption and 0.983 for desorption. For FDBD, the average R^2 values are 0.987 for adsorption and 0.999 for desorption. The PE (%) for the Peleg model is exceptionally low,

Parameter	Adsorption			Desorption		
	25 °C	35 °C	45 °C	25 °C	35 °C	45 °C
Peleg model						
C_1	0.29	0.46	0.32	0.06	0.11	0.74
C_2	3.82	3.76	3.19	− 0.43	− 0.13	3.23
C_3	0.29	0.46	0.32	0.32	1.13	0.08
C_4	3.82	3.76	3.19	1.22	3.67	0.15
GAB model						
X_m	11.03	18.94	17.24	0.18	0.13	0.11
C	0.00	0.00	0.01	18.76	15.76	3.68
K	0.82	0.78	0.72	0.87	0.96	0.97
BET model						
X_m	0.07	0.08	0.06	0.05	0.12	0.09
C	0.51	1.14	1.78	− 12.31	46.65	5.66
Halsey model						
A	0.08	0.08	0.05	0.01	0.12	0.09
B	0.71	0.91	1.00	1.97	1.18	1.08
Oswin model						
A	0.05	0.09	0.08	0.22	0.24	0.16
B	1.15	0.93	0.84	0.22	0.65	0.72
Smith model						
A	− 0.05	− 0.10	− 0.07	0.14	0.04	0.00
B	0.17	0.30	0.23	0.09	0.32	0.26
Adam and shove model						
A	0.03	0.02	0.05	0.21	0.14	1.00
B	− 0.29	− 0.19	− 0.51	− 0.61	0.06	− 0.95
C	0.45	0.04	1.16	1.72	− 0.75	0.89
D	0.30	0.99	− 0.11	− 1.01	1.76	− 0.83

Table 2. The estimated constants of the models applied to the actual adsorption and desorption data of VDBD at different temperatures.

with VDBD adsorption showing an average PE of 3.02%, and desorption at 0.04%. For FDBD, the average PE for adsorption is 1.91%, while desorption is at 0.02%, making it the most accurate model for both materials.

The GAB model performs reasonably well at higher temperatures, especially for FDBD, but faces challenges with VDBD at 25 °C. The average SSE for VDBD adsorption is 7.15×10^{-4} and desorption is 1.12×10^{-3} , while for FDBD, the average SSE is 6.98×10^{-4} for adsorption and 1.87×10^{-2} for desorption. The R^2 values for VDBD are 0.964 for adsorption and 0.992 for desorption, while for FDBD, these values are 0.984 for adsorption and 0.989 for desorption. The PE for the GAB model is relatively higher, especially for VDBD adsorption, with an average of 20.97%, and desorption at 1.06%. For FDBD, adsorption shows an average PE of 27.55%, and desorption is 6.62%, indicating a lower accuracy than the Peleg model.

The BET model provides reasonable fits for both VDBD and FDBD, though with higher error margins. The average SSE for VDBD adsorption is 1.37×10^{-3} and desorption is 2.01×10^{-2} , while for FDBD, the average SSE for adsorption is 1.08×10^{-3} and desorption is 1.92×10^{-2} . The R^2 for VDBD averages 0.939 for adsorption and 0.938 for desorption, while for FDBD, these values are 0.977 for adsorption and 0.967 for desorption. The PE for the BET model is noticeably higher, with an average of 26.61% for VDBD adsorption and 7.03% for desorption. For FDBD, adsorption shows an average PE of 50.16%, and desorption is at 5.98%, indicating that the BET model is less accurate than both the Peleg and GAB models.

The Halsey model shows poor fits for both adsorption and desorption, with VDBD exhibiting high SSE values (1.10×10^{-2}) and low R^2 (0.923 for adsorption, 0.937 for desorption). For FDBD, the average SSE is 1.03×10^{-2} . The PE for VDBD averages 44.85% for adsorption and 6.46% for desorption, while for FDBD, the PE averages 78.69% for adsorption and 5.27% for desorption, indicating the Halsey model's poor performance.

The Oswin model shows varied performance based on the material and temperature. The average SSE for VDBD adsorption is 1.29×10^{-3} and desorption is 1.91×10^{-2} , whereas for FDBD, the SSE values are 1.04×10^{-3} for adsorption and 1.82×10^{-2} for desorption. The R^2 for VDBD averages 0.942 for adsorption and 0.939 for desorption, while for FDBD, the R^2 values are 0.979 for adsorption and 0.932 for desorption. The PE for the Oswin model averages 28.78% for VDBD adsorption and 6.77% for desorption. For FDBD, the average PE for adsorption is 56.41% and 5.67% for desorption, suggesting that the Oswin model provides poor fit.

The Smith model shows poor fits overall. The average SSE for VDBD adsorption is 1.02×10^{-3} and desorption is 1.09×10^{-2} , while for FDBD, the SSE is 3.01×10^{-3} for adsorption and 1.6×10^{-2} for desorption. The average R^2 for VDBD is 0.953 for adsorption and 0.932 for desorption, while for FDBD, the values are 0.949 for adsorption and 0.903 for desorption. The PE for the Smith model averages 22.28% for VDBD adsorption and 5.45% for

Parameter	Adsorption			Desorption		
	25 °C	35 °C	45 °C	25 °C	35 °C	45 °C
Peleg model						
C_1	0.39	0.58	0.22	1.01	0.14	1.51
C_2	2.94	2.75	1.50	4.41	0.00	5.26
C_3	0.39	1.58	1.41	0.19	1.57	0.14
C_4	2.94	13.67	6.38	0.03	5.01	0.22
GAB model						
X_m	2.43	1.78	4.11	0.17	0.12	0.08
C	0.05	0.04	0.02	13.8	25.2	74.62
K	0.75	0.85	0.82	0.92	1.0	1.08
BET model						
X_m	0.08	0.09	0.11	0.18	0.12	0.12
C	1.66	0.88	1.18	25.3	26.15	3.48
Halsey model						
A	0.08	0.09	0.11	0.09	0.14	0.14
B	0.94	0.85	0.91	1.57	1.08	0.96
Oswin model						
A	0.10	0.09	0.12	0.27	0.23	0.19
B	0.88	1.01	0.95	0.46	0.72	0.83
Smith model						
A	-0.08	-0.11	-0.12	0.10	0.03	-0.01
B	0.29	0.34	0.40	0.26	0.33	0.33
Adam and Shove model						
A	0.01	-0.11	-0.14	0.15	0.08	0.03
B	-0.25	1.23	1.64	0.36	0.80	0.77
C	0.74	-3.62	-4.68	-1.39	-2.97	-2.63
D	0.24	3.67	4.59	-1.01	3.58	3.19

Table 3. The estimated constants of the models applied to the actual adsorption and desorption data of FDBD at different temperatures.

desorption. For FDBD, the PE is 25.36% for adsorption and 8.03% for desorption, indicating that the Smith model is not ideal for either material.

The Adam and Shove model provides good fits for both adsorption and desorption. The average SSE for VDBD adsorption is 8.94×10^{-5} and for desorption is 1.05×10^{-2} , while for FDBD, the SSE is 8.18×10^{-4} for adsorption and 1.69×10^{-2} for desorption. The R^2 values for VDBD average 0.994 for adsorption and 0.989 for desorption. For FDBD, the average R^2 is 0.982 for adsorption and 0.997 for desorption. The PE for the Adam and Shove model averages 3.15% for VDBD adsorption and 5.10% for desorption. For FDBD, the PE is 7.94% for adsorption and 7.25% for desorption, suggesting that this model provides good accuracy, especially for desorption.

Overall, among the models tested for adsorption and desorption of VDBD and FDBD, the Peleg model consistently outperforms the others across all parameters. It exhibits the lowest SSE values, the highest R^2 values, and the lowest. The R^2 values for the association between the experimental and predicted sorption data of VDBD and FDBD were 0.998 for adsorption and 0.995 for desorption. This is evidenced by the comparison between the experimental data and the values predicted by Peleg model, as presented in Fig. 4. Additionally, Figs. 5a-b clearly show that the Peleg model effectively described the experimental data for both the adsorption and desorption isotherms at different temperatures.

Although the other models, particularly the GAB and BET models, are widely applied to food sorption data due to their theoretical foundations, they showed limited accuracy in describing the full range of the sorption isotherms for Barhi dates, particularly at higher relative humidity levels. This may be attributed to their assumptions regarding monolayer adsorption, which may not fully capture the multilayer sorption, and complex interactions present in high-sugar, high-moisture fruit matrices. In contrast, the Peleg model, being empirical and more flexible, better accommodated the nonlinear behavior observed across the entire water activity range. This model was suitable for fitting the sorption data of different food materials investigated by^{14,15,37,45,46}.

Prediction of the safe storage moisture content

Water activity (a_w) is a key factor affecting microbial growth in food products, directly influencing their quality and storage stability. Ruan, et al.⁴⁷ noted that bacterial, yeast, and mold activities are suppressed at a_w values less than 0.7, whereas most microorganisms are effectively inhibited at a_w values less than 0.6.

Investigating the sorption isotherms of Barhi date is crucial for determining optimal storage conditions. These data also aid in designing and optimizing drying processes by identifying suitable moisture levels. In this

Parameter	Adsorption			Desorption		
	25 °C	35 °C	45 °C	25 °C	35 °C	45 °C
Peleg model						
SSE	2.29×10^{-4}	1.21×10^{-4}	2.11×10^{-4}	1.87×10^{-4}	4.78×10^{-3}	5.22×10^{-5}
R ²	1.00	0.997	0.991	0.958	0.995	0.997
PE (%)	2.32	3.61	3.12	0.06	0.04	0.02
GAB model						
SSE	5.58×10^{-4}	8.32×10^{-4}	7.54×10^{-4}	5.1×10^{-4}	2.6×10^{-3}	2.45×10^{-2}
R ²	0.943	0.980	0.969	0.995	0.996	0.984
PE (%)	18.09	27.36	17.45	1.21	1.78	0.20
BET model						
SSE	5.84×10^{-4}	1.76×10^{-3}	1.76×10^{-3}	2.00×10^{-2}	2.82×10^{-2}	1.22×10^{-2}
R ²	0.933	0.956	0.927	0.864	0.968	0.983
PE (%)	24.17	34.31	21.36	8.84	8.20	4.04
Halsey model						
SSE	8.49×10^{-4}	2.35×10^{-3}	2.03×10^{-3}	2.20×10^{-2}	2.73×10^{-2}	1.13×10^{-2}
R ²	0.913	0.942	0.915	0.860	0.964	0.986
PE (%)	29.87	70.01	34.68	9.06	7.17	3.16
Oswin model						
SSE	6.76×10^{-4}	1.69×10^{-3}	1.52×10^{-3}	2.07×10^{-2}	2.62×10^{-2}	1.05×10^{-2}
R ²	0.931	0.959	0.937	0.895	0.937	0.985
PE (%)	16.56	43.38	26.40	9.35	7.57	3.38
Smith model						
SSE	7.09×10^{-4}	1.60×10^{-3}	7.45×10^{-4}	3.97×10^{-4}	2.36×10^{-2}	8.68×10^{-3}
R ²	0.927	0.963	0.969	0.911	0.916	0.970
PE (%)	21.54	39.98	5.31	0.11	10.50	5.74
Adam and shove model						
SSE	1.43×10^{-4}	4.81×10^{-5}	7.68×10^{-5}	1.08×10^{-4}	2.34×10^{-2}	8.04×10^{-3}
R ²	0.985	0.999	0.997	0.976	0.995	0.997
PE (%)	5.70	3.08	0.67	0.05	10.00	5.25

Table 4. The statistical fitting criteria of the models were applied to experimental adsorption and desorption data of VDBD at different temperatures.

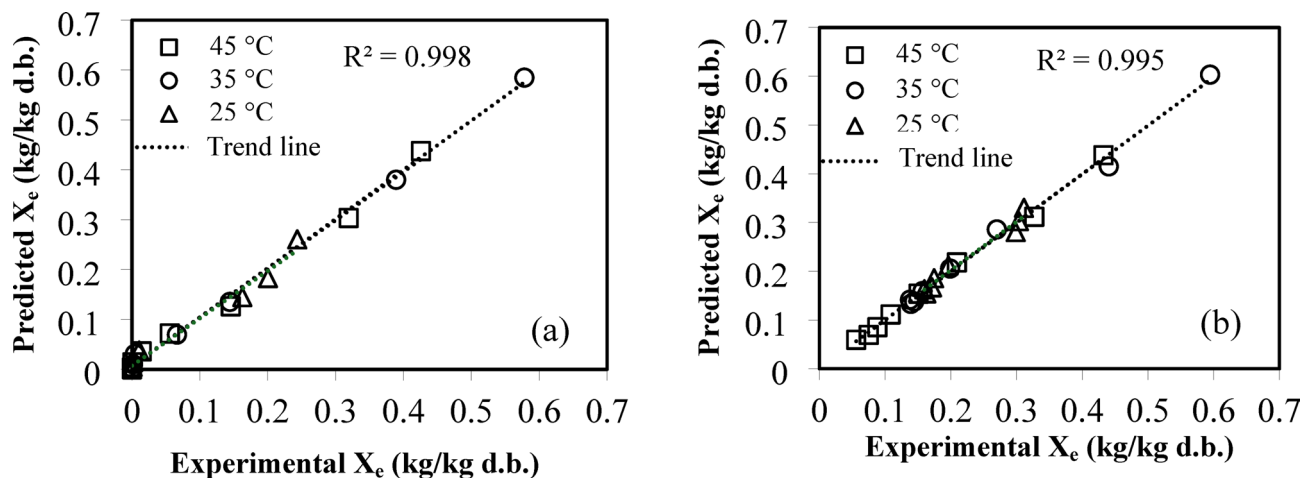


Fig. 4. Experimental and predicted equilibrium moisture content (X_e) during adsorption and (a) desorption (b) using Peleg model.

work, an a_w threshold of 0.6 was used to define the safe moisture content for VDBD and FDBD. Using the Peleg model, X_e values were estimated for storage temperatures of 25 °C, 35 °C, and 45 °C, with safe moisture contents of approximately 5%. Meanwhile, desorption isotherm data indicated that the optimal moisture level for drying VDBD was approximately 19%, across all studied temperatures. Additionally, for FDBD, X_e values were estimated

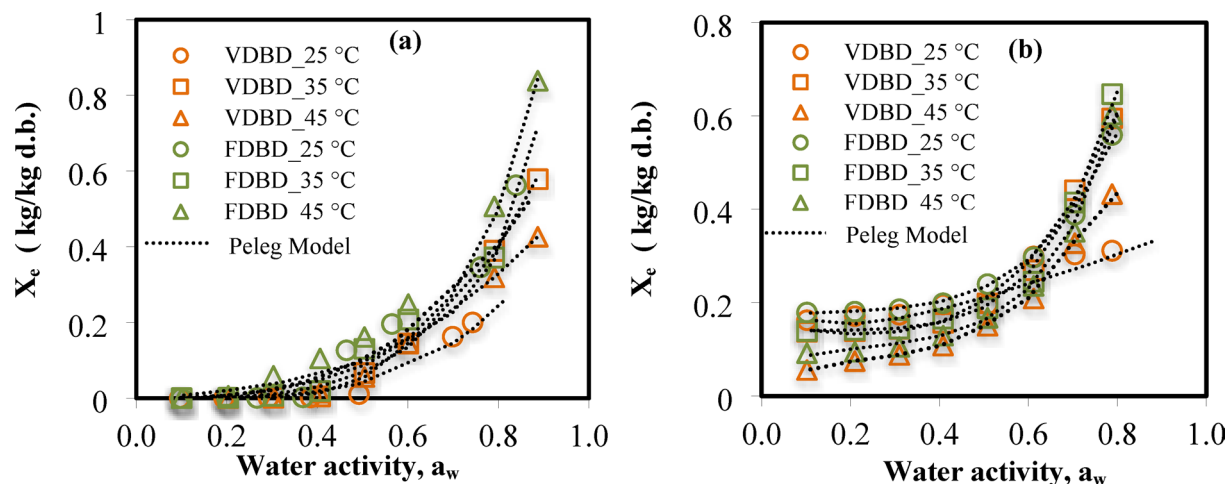


Fig. 5. Curves of the adsorption isotherms (a) and desorption isotherms (b) acquired for VDBD and FDBD at different temperatures (25, 35, and 45 °C).

at storage temperatures of 25 °C, 35 °C, and 45 °C, with a safe moisture content of approximately 9% for all tested temperatures. Moreover, the desorption isotherm data suggested that the optimal moisture content for drying FDBD was approximately 19% across all the studied temperatures. These outcomes suggest that FDBD has a higher moisture tolerance before it becomes susceptible to spoilage, but it also highlights the hygroscopic nature of FDBD, which can make it more sensitive to moisture fluctuations during storage. In contrast, VDBD, with its lower moisture content and stronger moisture binding properties, offers better stability against rehydration and microbial contamination, making it more suitable for long-term storage, especially under fluctuating ambient conditions.

Adsorption and desorption isotherms of VDBD and FDBD

The equilibrium moisture content (X_e) values of VDBD and FDBD at various temperatures (25, 35, and 45 °C) were plotted against water activity (a_w) to illustrate the adsorption and desorption isotherms (Figs. 5a–b). According to the standard classification of adsorption and desorption phases in food systems, illustrated in Figure (6), the adsorption isotherms follow Type III behavior with a concave upward shape. In Zone I ($a_w = 0–0.4$), moisture adsorption is minimal, whereas in Zone II ($a_w = 0.4–0.8$), water molecules cluster, gradually increasing moisture uptake. In Zone III ($a_w > 0.8$), capillary condensation causes a rapid increase in moisture retention⁴⁰. This curve shape is typical of foods with high sugar contents, which tend to absorb minimal water at low water activities and significant amounts at relatively high humidities⁴¹. However, the desorption isotherms illustrated in Fig. 5b for both VDBD and FDBD exhibit characteristics of Type V behavior, displaying a concave shape along with a pronounced hysteresis between the adsorption and desorption branches, as classified in Fig. 6. This characteristic is closely tied to the moisture removal mechanisms inherent in each drying method. In VDBD, water is removed through evaporation under reduced pressure and moderate heat, which can partially collapse cellular structures and reduce porosity. This structural alteration leads to reduced capillary pathways for moisture transport and a more restricted reabsorption of water, thereby contributing to the hysteresis observed in the isotherms. On the other hand, FDBD relies on sublimation to remove moisture directly from the frozen state, preserving the porous microstructure of the fruit. This intact porous network enhances moisture retention and rehydration capacity yet still displays hysteresis due to the binding of water within fine capillaries and porous matrices. The concave shape of the isotherms in both cases reflects the increasing difficulty of removing tightly bound water at lower water activities, while the hysteresis loop indicates structural differences during sorption and desorption, directly influenced by the drying-induced microstructural changes^{48,49}.

In terms of the effect of a_w on the adsorption isotherms, the results in Fig. 5a demonstrated that as a_w increases at a constant temperature, X_e in VDBD and FDBD also increases. At lower a_w levels (below 0.2), X_e remained minimal across all temperatures. However, once a_w exceeded 0.4, there was a significant increase in X_e , particularly at elevated temperatures. This phenomenon could be attributed to the fact that an increase in water activity leads to increased water vapor pressure in the air^{14,15}. As a result, water vapor moves into the VDBD and FDBD, which have lower vapor pressures, enhancing moisture adsorption. Conversely, in the context of the desorption isotherm (Fig. 5b), at any given temperature, as a_w decreases, X_e also decreases. This trend is consistent across all temperature levels, indicating that lower humidity levels lead to greater moisture release from the material. At lower a_w levels (below 0.2), the moisture content remains relatively low across all temperatures. However, as a_w surpasses 0.4, there is a notable increase in X_e , particularly at 35 °C. This behavior can be explained by the fact that when the water vapor pressure in the air increases, some of the water from the VDBD and FDBD, which has a lower vapor pressure, is released into the air, facilitating the desorption process^{14,15}. These trends are in agreement with those reported for different cultivars of dates^{31–34,43}.

The effect of temperature on X_e during adsorption varied depending on the drying technique applied to Barhi dates (Fig. 5a). In the case of VDBD, X_e generally increased with rising temperature at intermediate to high a_w

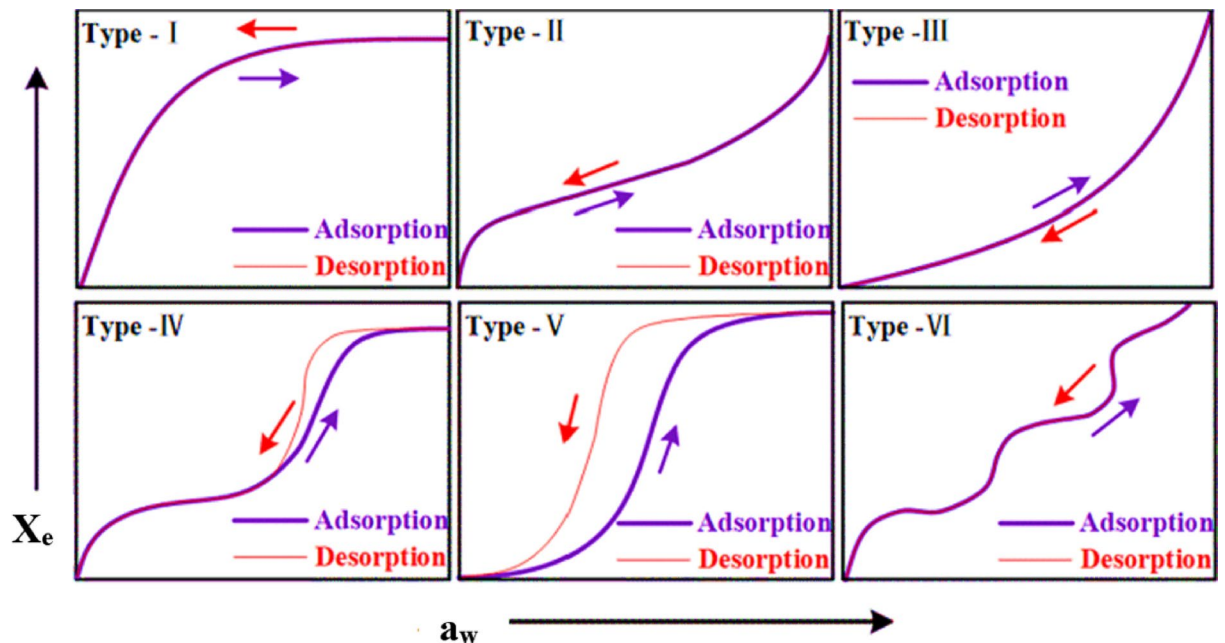


Fig. 6. Standard classifications of adsorption and desorption phases in food systems.

levels. For instance, at an a_w of approximately 0.4, X_e increased from 0.200 at 25 °C to 0.578 at 35 °C, followed by a slight decline to 0.426 at 45 °C. This non-linear behavior suggests that moderate temperatures may enhance water binding due to structural relaxation or pore reactivation, while higher temperatures could induce partial structural collapse or reduce surface hygroscopicity, limiting moisture uptake. Conversely, FDBD exhibited a more linear and pronounced increase in X_e across all a_w levels with rising temperature. At the highest a_w level, X_e rose from 0.562 at 25 °C to 0.712 at 35 °C and further to 0.839 at 45 °C, indicating that freeze-dried samples retained their porous structure and moisture-absorbing capacity even at elevated temperatures.

Regarding desorption, both VDBD and FDBD samples displayed a general decrease in X_e with increasing temperature, particularly at lower a_w values (≤ 0.6), as shown in Fig. 5b. In VDBD, X_e consistently declined as temperature increased from 25 °C to 45 °C, reflecting reduced moisture retention capacity due to increased molecular mobility and weakened water–matrix interactions. However, a deviation from this trend was observed at the highest a_w level, where X_e initially increased from 0.311 at 25 °C to 0.595 at 35 °C, before dropping to 0.432 at 45 °C. This anomaly could be attributed to the complex interactions between temperature, a_w , and matrix structure, which may temporarily enhance water retention before the thermal effects dominate. FDBD samples followed a similar pattern, with X_e increasing from 0.559 at 25 °C to 0.646 at 35 °C, and then slightly decreasing to 0.603 at 45 °C. Though less pronounced than in VDBD, this trend still aligns with the typical temperature-induced reduction in water-binding strength, reinforcing the thermodynamic nature of desorption processes in dried food systems. This effect of temperature on sorption isotherms is linked to thermodynamic theory, as suggested by Hossain, et al.⁴².

Regards the effect of drying methods on sorption isotherm, the sorption isotherms for both VDBD and FDBD followed Type III sigmoidal patterns for adsorption phase and Type V for desorption phase, typical of high-sugar food products (Figs. 5a–b). However, significant differences in X_e were observed between the two drying methods across varying temperatures. At a given a_w , FDBD generally exhibited higher X_e compared to VDBD, indicating a higher capacity for moisture retention. For instance, at $a_w \approx 0.9$, FDBD showed an X_e of 0.56 g/g (25 °C) and 0.84 g/g (45 °C), whereas VDBD had lower X_e values of 0.20 g/g (25 °C) and 0.43 g/g (45 °C). These findings suggest that FDBD, due to its more porous structure formed during freeze-drying, is more hygroscopic than VDBD, which has a denser matrix resulting from vacuum drying at higher temperatures.

Moisture sorption hysteresis

Moisture sorption hysteresis refers to the phenomenon where the moisture content of a material at a given a_w differs depending on whether the material is undergoing adsorption (gaining moisture) or desorption (losing moisture). Specifically, hysteresis occurs when the moisture adsorption and desorption curves do not overlap, indicating that the material retains more moisture during desorption than during adsorption at the same a_w ¹¹. This behavior is clearly demonstrated in Figs. 7a–c, where the X_e values during desorption were consistently higher than those during adsorption across all a_w levels and temperatures. Moisture sorption hysteresis arises from differences in the adsorption and desorption mechanisms of porous materials. During adsorption, water molecules gradually bind to the material surface and accumulate within its pores through multilayer adsorption and capillary condensation. However, during desorption, water release is restricted by capillary forces, pore structure, and surface interactions, leading to moisture retention in smaller pores or strongly bound sites. As a result, water in the pores of a material requires more energy to evaporate because of capillary attraction.

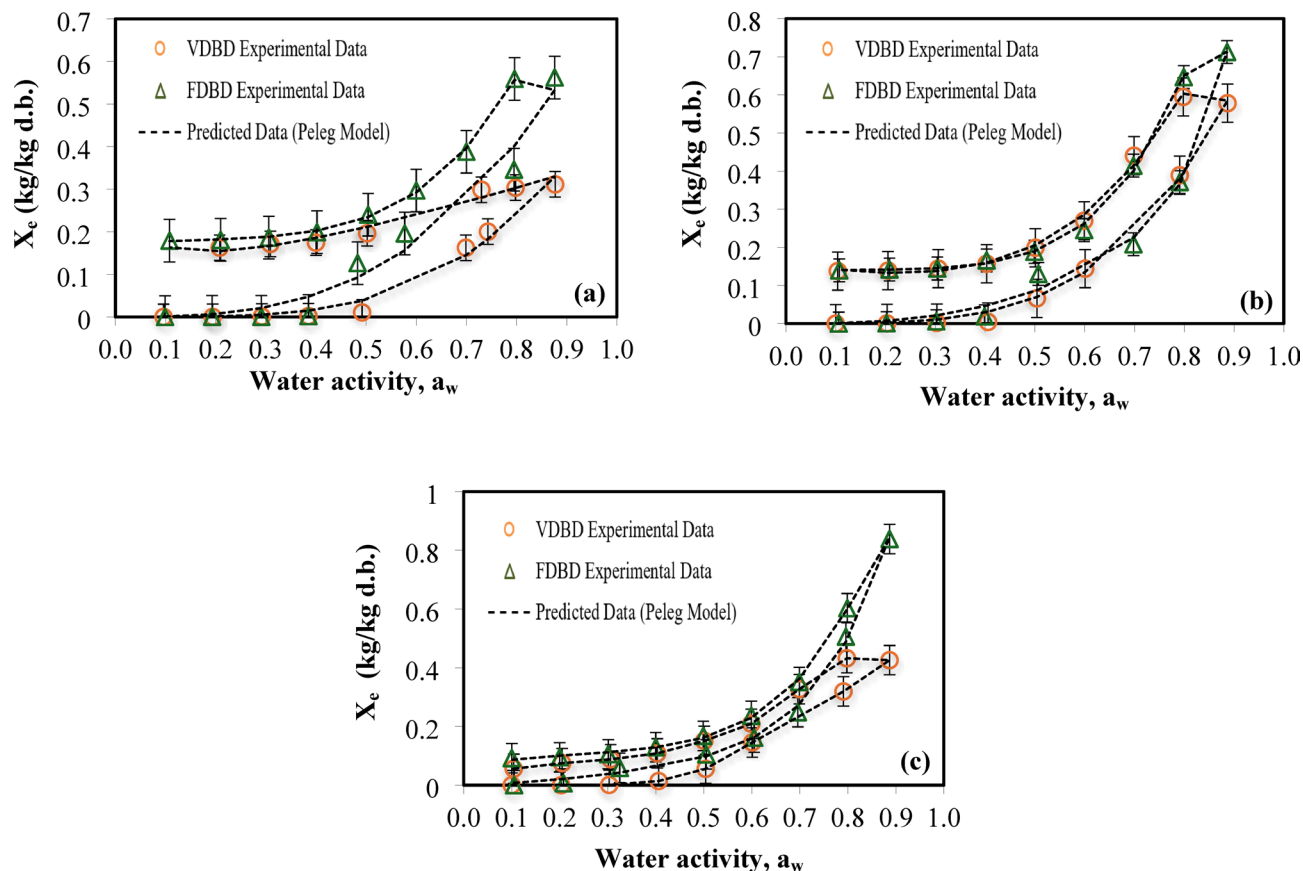


Fig. 7. Sorption hysteresis loops obtained for VDBD and FDBD at different temperatures: 25 °C (a), 35 °C (b), and 45 °C (c).

Consequently, X_e values during desorption remain consistently higher than those observed during adsorption. This phenomenon was detected for various food materials and reported by Fikry and Al-Awaadh¹¹, Fikry, et al.¹⁴, Treeamnuak, et al.¹⁵.

Moreover, the results revealed distinct trends in the effect of temperature on hysteresis. At 25 °C, the hysteresis values are generally greater, indicating that at lower temperatures, the material retains more water during desorption. This suggests stronger binding interactions between the material and water molecules, as lower temperatures decrease the kinetic energy of water molecules, making it harder for them to escape during desorption. As the temperature increased to 35 °C, the hysteresis values decreased slightly, implying a diminished ability of the material to retain water during desorption due to increased molecular motion, which facilitates the release of water molecules. At the highest temperature, 45 °C, the hysteresis values are the lowest. This significant reduction may be attributed to the increased temperature, which energizes water molecules, allowing them to break free from their sorption sites and consequently lowering X_e ⁴⁴. This trend is in agreement with that reported by Treeamnuak, et al.¹⁵, Mallek-Ayadi, et al.⁴⁵.

On the other hand, hysteresis behavior was more pronounced in FDBD than in VDBD. This was particularly evident at higher relative humidity (RH), where FDBD showed a larger gap between adsorption and desorption values. For example, at $a_w \approx 0.79$ and 25 °C, the desorption X_e for FDBD was 0.559 g/g, while the adsorption X_e was 0.346 g/g, yielding a hysteresis of 0.213 g/g. In contrast, VDBD exhibited a much smaller hysteresis of 0.148 g/g. This greater hysteresis in FDBD can be attributed to its more open and porous structure, which traps moisture more effectively during desorption. This characteristic could pose challenges during storage, particularly in fluctuating environmental conditions, where FDBD may absorb moisture more readily, leading to potential texture degradation and reduced shelf-life.

Thermodynamic properties of sorption isotherms

The thermodynamic properties that characterize the interaction between water and the food matrix are essential for assessing energy demands in drying and concentration processes. They play a crucial role in optimizing drying process design and determining ideal storage conditions to ensure the long-term stability of dried foods¹⁴. Thermodynamic properties, such as the differential heat of sorption, are crucial for understanding the intricate relationship between food materials and moisture. This parameter indicates that the energy changes during the sorption process, indicating how the energy requirements fluctuate as the food material interacts with water molecules at various moisture levels⁴⁴.

The isosteric heat of sorption or differential enthalpy values play a vital role in energy assessments. Q_{st} reflects the strength of intermolecular forces between water vapor and sorption sites. Variations in Q_{st} indicate that energy shifts occur as water molecules interact with the sorbent during sorption⁵⁰.

The concept of isosteric heat differs on the basis of whether it pertains to adsorption or desorption isotherms. During adsorption, it refers to the amount of energy released when water molecules bind to a material, although this energy is often minimal and difficult to quantify. Conversely, in desorption, it signifies the energy necessary to retain water within the substrate, representing the extra heat—beyond the latent heat of vaporization of pure water—required to break the molecular bonds between water and the material during dehydration.

Figure 8a illustrates the relationship between X_e and the Q_{st} of adsorption and desorption for VDBD. The results demonstrated an inverse trend, where a decrease in X_e corresponds to an increase in Q_{st} . During the adsorption process, as X_e increases, Q_{st} decreases slightly from 43.62 to 42.01 kJ/mol, indicating a reduction in the energy required for adsorption as the system becomes more hydrated. Similarly, during the desorption process, as X_e decreases from 0.457 to 0, Q_{st} increases slightly from 41.42 to 43.56 kJ/mol, suggesting that more energy is required to remove water molecules as the system becomes drier. Notably, the sorption heat is significantly greater at lower moisture levels, indicating strong molecular interactions between water and the food matrix, resulting in the formation of a monolayer. As a result, considerable energy is required to remove these tightly bound water molecules. Generally, desorption requires higher energy input compared to adsorption due to the stronger binding of water molecules within the food matrix. During desorption, energy is needed to overcome the forces holding water molecules in sorption sites, especially at low moisture levels where water is more tightly bound. In contrast, adsorption occurs more readily as water vapor interacts with available active sites, particularly in porous and low-moisture materials. This distinction has now been emphasized to highlight the thermodynamic implications of each process and their relevance to moisture management in food preservation. These findings are consistent with prior studies on various food products investigated by Fikry, et al.¹⁴, Lehmad, et al.³⁷, Yogendrarajah, et al.⁴⁴, Mallek-Ayadi, et al.⁴⁵. The correlations between Q_{st} and X_e are listed in Table 6.

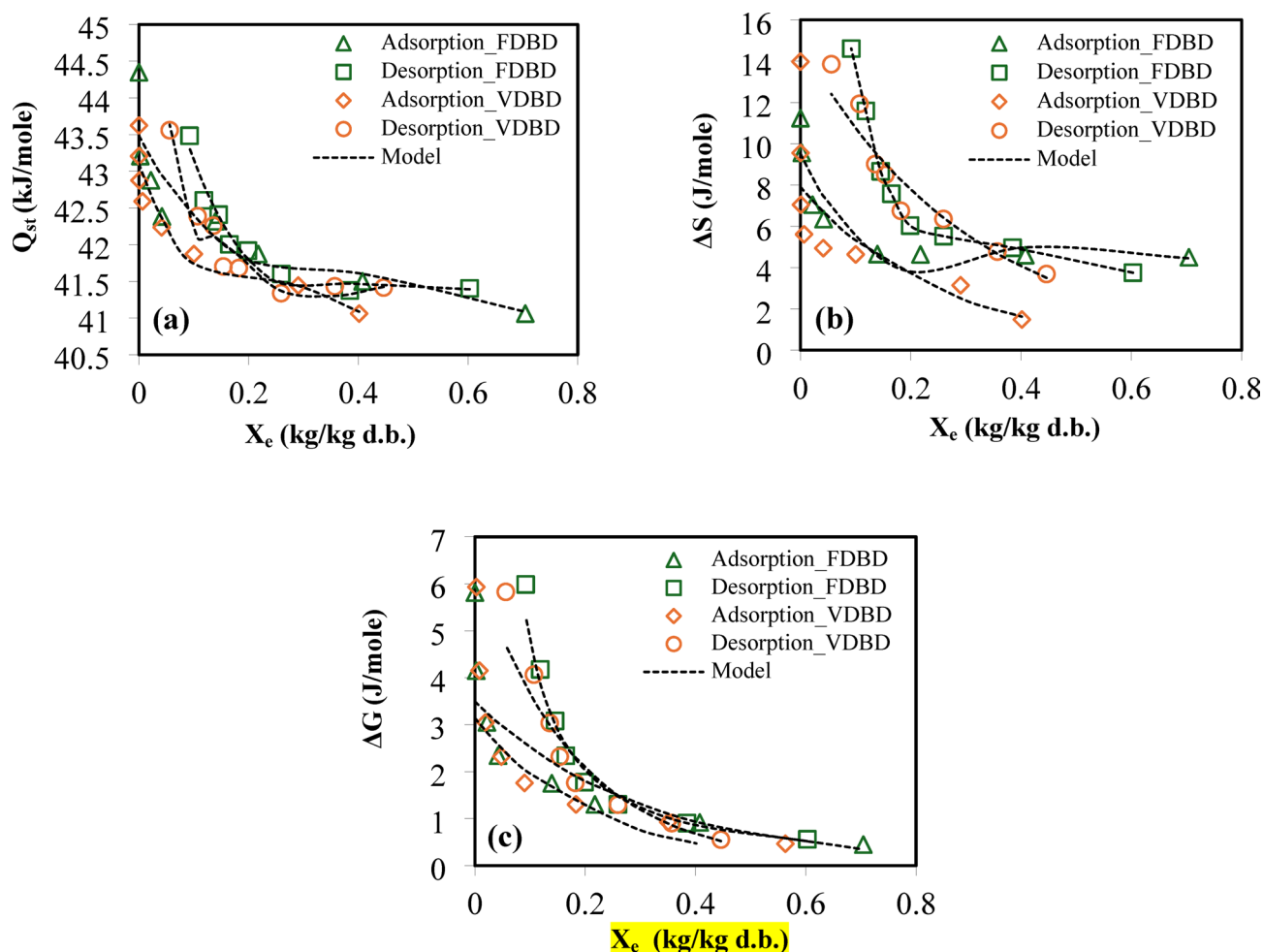


Fig. 8. Plots of the isosteric heat of sorption (a), differential entropy (b) and Gibbs free energy (c) against the equilibrium moisture content (X_e) of VDBD and FDBD.

Parameter	Adsorption			Desorption		
	25 °C	35 °C	45 °C	25 °C	35 °C	45 °C
Peleg model						
SSE	1.14×10^{-3}	3.84×10^{-4}	1.75×10^{-4}	1.84×10^{-5}	6.91×10^{-5}	3.90×10^{-5}
R ²	0.97	0.993	0.998	0.999	0.998	0.999
PE (%)	2.32	2.82	0.58	0.01	0.02	0.02
GAB model						
SSE	1.27×10^{-3}	5.12×10^{-4}	3.13×10^{-4}	4.7×10^{-3}	4.4×10^{-1}	6.01×10^{-3}
R ²	0.966	0.991	0.996	0.994	0.958	0.996
PE (%)	75.63	6.06	0.95	2.43	14.69	3.29
BET model						
SSE	1.70×10^{-3}	6.59×10^{-4}	8.84×10^{-4}	8.4×10^{-2}	2.46×10^{-2}	7.01×10^{-3}
R ²	0.956	0.988	0.988	0.993	0.959	0.974
PE (%)	137.88	10.49	2.12	3.72	7.17	2.66
Halsey model						
SSE	2.21×10^{-3}	1.09×10^{-3}	1.42×10^{-3}	2.58×10^{-2}	2.50×10^{-2}	6.50×10^{-2}
R ²	0.945	0.98	0.981	0.953	0.959	0.988
PE (%)	235.86	22.24	4.98	7.68	6.40	1.71
Oswin model						
SSE	1.63×10^{-3}	6.71×10^{-4}	8.29×10^{-4}	2.41×10^{-2}	2.40×10^{-2}	6.53×10^{-3}
R ²	0.959	0.988	0.989	0.902	0.924	0.969
PE (%)	155.53	11.43	2.26	7.57	6.96	2.49
Smith model						
SSE	1.14×10^{-3}	3.23×10^{-3}	4.67×10^{-3}	1.93×10^{-3}	2.05×10^{-2}	8.13×10^{-3}
R ²	0.967	0.942	0.938	0.92	0.879	0.909
PE (%)	54.59	16.89	4.59	7.26	9.40	7.44
Adam and shove model						
SSE	9.38×10^{-4}	1.16×10^{-3}	3.52×10^{-4}	2.10×10^{-2}	2.34×10^{-2}	6.44×10^{-3}
R ²	0.971	0.979	0.995	0.998	0.997	0.996
PE (%)	14.58	6.89	2.37	8.49	9.09	4.16

Table 5. The statistical fitting criteria of the models were applied to experimental adsorption and desorption data of FDBD at different temperatures.

The drying method significantly influences Q_{st} for both adsorption and desorption processes. For FDBD, Q_{st} decreases progressively from 44.35 kJ/mol to 41.06 kJ/mol, while the desorption values increase from 41.40 kJ/mol to 43.48 kJ/mol. This trend suggests that FDBD leads to a reduction in the energy required for adsorption over successive measurements, possibly due to the removal of loosely bound water molecules, which decreases the material's affinity for further adsorption. Conversely, the increasing desorption values indicate that more energy is needed to remove adsorbed molecules as the process continues, likely due to stronger interactions between the adsorbate and the adsorbent surface after initial drying.

In comparison, VDBD exhibits a similar but slightly moderate trend. The adsorption Q_{st} values decline from 43.62 kJ/mol to 41.06 kJ/mol, while desorption values rise from 41.42 kJ/mol to 43.56 kJ/mol. The initial adsorption heat for VDBD is lower than that of FDBD, suggesting that vacuum drying may partially reduce surface hydrophilicity or porosity, leading to weaker initial adsorption interactions. However, the desorption behavior closely mirrors that of FDBD, reinforcing that both methods ultimately strengthen adsorbate-adsorbent interactions over time.

ΔS measures the level of randomness in the water-sorbent system, offering valuable insights into processes such as dissolution, crystallization, and swelling. Figure 8b shows the correlation between ΔS and X_e for both the adsorption and desorption isotherms of VDBD and FDBD.

The results indicated a solid dependence of the ΔS values on X_e . Specifically, the adsorption phase has a lower entropy variation than does desorption, implying that water molecules are more mobile through desorption than through adsorption. During adsorption, ΔS decreases for both methods, indicating that the adsorbed water layers become more structured over time. However, the rate of this decrease differs: VDBD exhibits a sharper drop in ΔS (from 13.98 to 1.48 J/mol) compared to FDBD (11.24 to 4.50 J/mol), suggesting that vacuum drying leads to a more rapid loss of adsorbate mobility, likely due to a more uniform surface after initial moisture removal. In contrast, desorption ΔS increases over time for both methods, demonstrating that removing water becomes increasingly entropically unfavorable as stronger binding sites dominate. Here, FDBD ends with a slightly higher desorption ΔS (14.61 J/mol) than VDBD (13.85 J/mol), implying that freeze-dried samples retain more disordered residual water, making desorption slightly more thermodynamically demanding. Similar trends were reported by Fikry, et al.¹⁴, Lehmad, et al.³⁷, Yogendrarajah, et al.⁴⁴. ΔS is influenced by the strength

Property	Model	Constants*	VDBD		FDBD	
			Adsorption	Desorption	Adsorption	Desorption
Net isosteric heat of sorption (Q_{st})	Cubic $Q_{st} = a + b_1 (X_e) + b_2 (X_e)^2 + b_3 (X_e)^3$	a	43.10	45.32	43.49	45.92
		b_1	- 21.19	- 36.81	- 14.32	- 36.20
		b_2	87.09	110.16	35.20	92.99
		b_3	- 116.67	-106.07	- 27.97	- 75.31
		R^2	0.909	0.977	0.837	0.964
Differential entropy (ΔS)	Exponential $Q_{st} = a.e^{b.X_e}$	a	7.91	14.88	ND*	ND
		b	- 3.95	- 3.24	ND	ND
		R^2	0.80	0.94	ND	ND
	Cubic $Q_{st} = a + b_1 (X_e) + b_2 (X_e)^2 + b_3 (X_e)^3$	a	ND	ND	9.52	29.22
		b_1	ND	ND	- 56.05	- 210.97
		b_2	ND	ND	166.20	575.56
		b_3	ND	ND	- 137.49	- 490.44
		R^2	ND	ND	0.851	0.986
Gibbs free energy (ΔG)	Exponential $Q_{st} = a.e^{b.X_e}$	a	3.14	6.43	3.49	ND
		b	- 4.72	- 5.63	-3.29	ND
		R^2	0.811	0.952	0.901	ND
	Power $Q_{st} = a.(X_e)^b$	a	ND	ND	ND	0.278
		b	ND	ND	ND	- 1.237
		R^2	ND	ND	ND	0.979

Table 6. Mathematical models that adequately describe the thermodynamic properties of the adsorption and desorption of VDBD and FDBD. *a, b, b_1 , b_2 and b_3 are the constants of mathematical models (dimensionless). *ND means that the parameters were not determined.

of the molecular interactions in the system and the structural organization at the water–sorbent interface. These findings support the notion that lower ΔS values are associated with limited molecular movement when the material has an extreme moisture content. The relationship between the ΔS variation and X_e was effectively modeled via the models presented in Table 6.

ΔG serves as a key parameter in assessing the interaction between water molecules and the sorbent matrix. It also determines whether the sorption process occurs spontaneously or requires external energy input on the basis of the sign of ΔG —negative values indicate spontaneity, whereas positive values suggest a nonspontaneous process⁵¹. As shown in Fig. 8c, the ΔG values for VDBD and FDBD confirmed that both moisture adsorption and desorption were nonspontaneous processes, as indicated by their positive values.

This aligns with the fundamental nature of sorption, which necessitates energy input, classifying it as an endergonic reaction^{13,51}. Similar trends were observed in previous studies^{13,51}.

Moreover, the results revealed that as X_e decreased, the ΔG values increased. Figure 8c shows that in the case of adsorption, ΔG decreases from 5.93 to 0.47 kJ/mol, reflecting a decrease in the spontaneity of the adsorption process as the moisture content increases, suggesting that moisture uptake became energetically more favorable at higher moisture contents. This is likely due to the initial presence of more active binding sites and lower resistance to moisture diffusion. For desorption, ΔG increases from 0.55 to 5.83 kJ/mol, indicating that desorption becomes less spontaneous as X_e decreases. This pattern suggests that desorption demands more energy than adsorption, particularly in the low-moisture range, where water is strongly bound to the matrix through hydrogen bonding or capillary forces. These trends are in agreement with those previously reported by Fikry, et al.¹⁴,Yogendrarajah, et al.⁴⁴.

When comparing the two drying methods, FDBD samples consistently exhibited lower ΔG values across most X_e levels than VDBD samples, indicating that moisture sorption is more thermodynamically favorable in freeze-dried samples. This can be attributed to the open porous structure and higher surface area generated by sublimation during freeze-drying, which facilitates easier water molecule diffusion and interaction. On the other hand, the denser, collapsed structure of vacuum-dried samples imposes higher energetic barriers for water transport, resulting in greater ΔG values and reduced sorption efficiency. The regression lines in Fig. 8c illustrate these relationships with high predictive accuracy ($R^2 > 0.92$), as described by the equations in Table 6. This comparative thermodynamic insight underscores how drying method significantly influences the energy dynamics of sorption behavior, which is critical in optimizing drying processes and storage stability of dried date products.

Conclusion

To conclude, the study successfully characterized the moisture sorption isotherms of VDBD and FDBD across a range of temperatures and water activity levels using a DVS apparatus. The observed Type III and Type V isotherm behaviors for adsorption and desorption, respectively, reflect distinct moisture interaction mechanisms, with adsorption increasing with water activity and desorption showing the opposite trend, indicating strong hysteresis—a sign of structural and binding changes during moisture exchange. The Peleg model's high accuracy

in fitting the data across all conditions confirms its reliability for predicting moisture behavior in both drying methods, supporting its use in industrial modeling and control. The recommended safe moisture contents of 5% for VDBD and 9% for FDBD provide practical guidance for minimizing spoilage risks during storage. The thermodynamic analysis revealed that as equilibrium moisture content (X_e) decreased, the isosteric heat of sorption (Q_{st}), entropy (ΔS), and Gibbs free energy (ΔG) increased, indicating stronger moisture binding at lower moisture levels. These parameters were also found to be predictable as functions of X_e , enabling better estimation of energy requirements and storage dynamics. The nonspontaneous nature of sorption processes suggests that external energy input is essential for moisture transfer, especially in low-humidity environments, which is important for designing efficient drying and storage systems. These findings offer crucial insights for optimizing drying protocols, packaging materials, and storage environments, ultimately enhancing the stability and shelf life of VDBD and FDBD. Food manufacturers can apply these results to prevent microbial growth, maintain product quality, and improve energy efficiency during processing.

However, the study faced limitations due to the inability to perform Scanning Electron Microscopy (SEM) and proximate composition analysis, restricting insights into microstructure and nutritional content due to methodological constraints. Future research should include these analyses and use larger datasets to enhance understanding and optimize processing techniques.

Data availability

Data is provided within the manuscript.

Received: 19 February 2025; Accepted: 9 May 2025

Published online: 05 June 2025

References

1. Abu-Shama, H. S., Abou-Zaid, F. O. F. & El-Sayed, E. Z. Effect of using edible coatings on fruit quality of Barhi date cultivar. *Sci. Hort.* **265**, 109262. <https://doi.org/10.1016/j.scienta.2020.109262> (2020).
2. Morsy, M. K. Effect of enzymatic extraction method on quality parameters and sensory acceptability of date dabs produced from second grade dates. *Annals Agricultural Sci. Moshtohor*. **60**, 53–62. <https://doi.org/10.21608/assj.2022.227246> (2022).
3. Mehyar, G. F., Assi, E., Alsmairat, N. M., Holley, R. A. & N. G. & Effect of edible coatings on fruit maturity and fungal growth on B Erhi dates. *Int. J. Food Sci. Technol.* **49**, 2409–2417. <https://doi.org/10.1111/ijfs.12562> (2014).
4. Alsawmahi, O. N. et al. Phenolic, tannin, antioxidant, color, and sensory attributes of Barhi date (*Phoenix dactylifera*) fruit stored in modified atmosphere packages. *J. Food Biochem.* **42**, e12576. <https://doi.org/10.1111/jfbc.12576> (2018).
5. Alhamdan, A. M., Elkhair, D. O. & Ehmed, K. A. Modeling of respiration rate of fresh date fruits (Barhi cultivar) under aerobic conditions. *J. Adv. Agricultural Technol.* **2** <https://doi.org/10.12720/joaat.2.2.120-124> (2015).
6. Jomlaperatikul, P. et al. Effect of sample pretreatment and drying methods on quality of dates. *KKU Res. J. (Graduate Studies)*. **23**, 120–129 (2023).
7. Ahmed, K. A. & Ashmawy, N. M. E. Color stability of Freeze-dried date fruits (Barhi CV.) during storage. *Adv. Res.* **8**, 1–9. <https://doi.org/10.9734/AIR/2016/31168> (2017).
8. Alhamdan, A., Hassan, B., Alkahtani, H., Abdelkarim, D. & Younis, M. Freezing of fresh Barhi dates for quality preservation during frozen storage. *Saudi J. Biol. Sci.* **25**, 1552–1561. <https://doi.org/10.1016/j.sjbs.2016.02.003> (2018).
9. Selim, M., Nagy, K. & Hamed, M. Influence of packaging and cold storage conditions on the Physio-chemical properties of Barhi date fruits. *Assiut J. Agricultural Sci.* **51**, 79–91. <https://doi.org/10.21608/ajas.2020.104165> (2020).
10. Al-Kaabi, H. J. Effect of modified atmosphere packaging on quality of Barhi dates at Khalal stage. *Int. J. Food Stud.* **9** <https://doi.org/10.7455/ijfs/9.SI.2020.a10> (2020).
11. Fikry, M. & Al-Awaadh, A. M. Characteristics of dynamics sorption isotherms of date flesh powder rich in fiber. *Int. J. Food Eng.* **12**, 469–480. <https://doi.org/10.1515/ijfe-2015-0223> (2016).
12. Van den Berg, C. *Vapour sorption equilibria and other water-starch interactions: A physico-chemical approach* PhD thesis, Agricultural University (1981).
13. Hassan, B., Mustapha, A. T., Al-Awaadh, A. M. & Ahmed, K. A. Physical and moisture sorption thermodynamic properties of Sukkari date (*Phoenix dactylifera* L.) powder. *CyTA-Journal Food*. **18**, 264–273. <https://doi.org/10.1080/19476337.2020.1738558> (2020).
14. Fikry, M. et al. Sorption isotherms and thermodynamic characteristics of gelatin powder extracted from Whitefish skin: mathematical modeling approach. *Foods* **13**, 92. <https://doi.org/10.3390/foods13010092> (2023).
15. Treamnuk, T., Pengprakhon, T. & Treamnuk, K. Effect of temperature on moisture sorption isotherm characteristics of Thai Jasmine paddy (Khao Dawk Mali 105). *LWT* **210**, 116871. <https://doi.org/10.1016/j.lwt.2024.116871> (2024).
16. Collazos-Escobar, G. A., Hurtado-Cortés, V. & Bahamón-Monje, A. F. Gutiérrez-Guzmán, N. Mathematical modeling of water sorption isotherms in specialty coffee beans processed by wet and semidry postharvest methods. *Sci. Rep.* **15**, 3898. <https://doi.org/10.1038/s41598-024-83702-y> (2025).
17. Al-Muhtaseb, A. H., McMinn, W. A. M. & Magee, T. R. A. Water sorption isotherms of starch powders. *J. Food Eng.* **61**, 297–307. [https://doi.org/10.1016/s0260-8774\(03\)00133-x](https://doi.org/10.1016/s0260-8774(03)00133-x) (2004).
18. Bingol, G., Prakash, B. & Pan, Z. Dynamic vapor sorption isotherms of medium grain rice varieties. *LWT - Food Sci. Technol.* **48**, 156–163. <https://doi.org/10.1016/j.lwt.2012.02.026> (2012).
19. Antonioli, P. R., Ferrari, C. C., Borges, D. F. & Germer, S. P. M. Sorption isotherms, glass transition and storage stability of drum-dried Mango peels obtained with and without process additives. *Drying Technol.* **41**, 378–389. <https://doi.org/10.1080/07373937.2022.2093897> (2023).
20. Sormoli, M. E. & Langrish, T. A. Moisture sorption isotherms and net isosteric heat of sorption for spray-dried pure orange juice powder. *LWT-Food Sci. Technol.* **62**, 875–882. <https://doi.org/10.1016/j.lwt.2014.09.064> (2015).
21. Peleg, M. Assessment of a semi-empirical four parameter general model for sigmoid moisture sorption isotherms. *J. Food Process Eng.* **16**, 21–37. <https://doi.org/10.1111/j.1745-4530.1993.tb00160.x> (1993).
22. Oswin, C. R. The kinetics of package life III. The isotherm. *J. Chem. Ind.* **65**, 419–421. <https://doi.org/10.1002/jctb.5000651216> (1946).
23. Chen, C. S. Equilibrium moisture curves for biological materials. *Trans. ASEA.* **14**, 924–926. <https://doi.org/10.13031/2013.38421> (1971).
24. Halsey, G. Physical adsorption on non-uniform surfaces. *J. Chem. Phys.* **16**, 931–937. <https://doi.org/10.1063/1.1746689> (1948).
25. Iglesias, H. A. & Chirife, J. Prediction of the effect of temperature on water sorption isotherms of food material. *J. Food Technol.* **11**, 109–116 (1976c).

26. Brunauer, S., Emmett, P. H. & Teller, E. Adsorption of gases in multimolecular layers. *J. Am. Chem. Soc.* **60**, 309–320. <https://doi.org/10.1021/ja01269a023> (1938).
27. Smith, S. E. The sorption of water vapour by high polymers. *J. Am. Chem. Soc.* **69**, 646. <https://doi.org/10.1021/ja01195a053> (1947).
28. Henderson, S. M. A basic concept of equilibrium moisture. *Agricultural Eng.* **33**, 29–32 (1952).
29. Khater, E. S. Effect of drying systems on the parameters and quality of dried Basil. *Annals Agricultural Sci. Moshtohor*. **58**, 261–272. <https://doi.org/10.21608/assjm.2020.112760> (2020).
30. Chirife, J. & Iglesias, H. A. Equations for fitting water sorption isotherms of foods. Part I. A review. *J. Food Technol.* **13**, 159–174. <https://doi.org/10.1111/j.1365-2621.1978.tb00792.x> (1978).
31. Mediani, A. et al. The isothermal sorption measurement and the isosteric heats determinations for the South Algerian date varieties. *Instrum. Mesure Métrologie*. **18**, 389–396. <https://doi.org/10.18280/im.180408> (2019).
32. Moitte, S. A. & Heikal, Y. Sorption isotherms behaviour of some Egyptian date fruit varieties. (2013). <https://doi.org/10.5555/20143024908>
33. Knani, S. et al. STERIC AND ENERGETIC INTERPRETATIONS. *JP J. Biostatistics*. **24**, 309–333. <https://doi.org/10.17654/0973514324019> (2024).
34. Ferradji, A. & Matallah, M. Sorption isotherms and isosteric heats for Algerian dates Deglet nour. *Am. J. Food Technol.* **7**, 352–362. <https://doi.org/10.3923/ajft.2012.352.362> (2012).
35. AOAC. *Official Methods of Analysis of AOAC International* Vol. 17 (AOAC international, 2000).
36. Quirijns, E. J., Van Boxtel, A. J., van Loon, W. K. & Van Straten, G. Sorption isotherms, GAB parameters and isosteric heat of sorption. *J. Sci. Food. Agric.* **85**, 1805–1814. <https://doi.org/10.1002/jsfa.2140> (2005).
37. Lehmad, M., Hachimi, E. L., Lhomme, Y., Mghazli, P., Abdenouri, N. & S. & Comprehensive analysis of Adsorption–Desorption isotherms, drying kinetics, and nutritional quality of black soldier fly (*Hermetia illucens*) larvae. *Food Biophys.* **19**, 938–954. <https://doi.org/10.1007/s11483-024-09867-1> (2024).
38. Bahloul, N., Boudhrioua, N. & Kechaou, N. Moisture desorption–adsorption isotherms and isosteric heats of sorption of Tunisian Olive leaves (*Olea Europaea* L). *Ind. Crops Prod.* **28**, 162–176. <https://doi.org/10.1016/j.indcrop.2008.02.003> (2008).
39. Fikry, M. et al. Kinetics modelling of the colour, hardness, grinding energy consumption and oil yield changes during the conventional roasting of palm date seeds. *Food Sci. Technol. Res.* **25**, 351–362. <https://doi.org/10.3136/fstr.25.351> (2019).
40. Caballero-Cerón, C., Guerrero-Beltrán, J., Mújica-Paz, H., Torres, J. & Welti-Chanes, J. Moisture sorption isotherms of foods: experimental methodology, mathematical analysis, and practical applications. *Water Stress Biol. Chem. Pharm. Food Syst.* **187**–214. https://doi.org/10.1007/978-1-4939-2578-0_15 (2015).
41. Ocheme, O. B., Ariahu, C. C. & Kongo Ingbian, E. Moisture sorption characteristics of Dakuwa (Nigerian cereal/groundnut snack). *Int. J. Food Eng.* **9**, 499–504. <https://doi.org/10.1515/ijfe-2012-0242> (2013).
42. Hossain, M., Bala, B., Hossain, M. & Mondol, M. Sorption isotherms and heat of sorption of pineapple. *J. Food Eng.* **48**, 103–107. [https://doi.org/10.1016/S0260-8774\(00\)00132-1](https://doi.org/10.1016/S0260-8774(00)00132-1) (2001).
43. Bellagha, S., Sahli, A. & Farhat, A. Desorption isotherms and isosteric heat of three Tunisian date cultivars. *Food Bioprocess Technol.* **1**, 270–275. <https://doi.org/10.1007/s11947-007-0006-1> (2008).
44. Yogendrarajah, P., Samapundo, S., Devlieghere, F., De Saeger, S. & De Meulenaer, B. Moisture sorption isotherms and thermodynamic properties of whole black peppercorns (*Piper nigrum* L). *LWT-Food Sci. Technol.* **64**, 177–188. <https://doi.org/10.1016/j.lwt.2015.05.045> (2015).
45. Mallek-Ayadi, S., Bahloul, N. & Kechaou, N. Mathematical modelling of water sorption isotherms and thermodynamic properties of Cucumis melo L. seeds. *Lwt* **131**, 109727. <https://doi.org/10.1016/j.lwt.2020.109727> (2020).
46. Efendi, M. Analysis of Courie-GAB-Peleg models and neural networks in jelly candy by corn starch: drying kinetic and moisture sorption isotherms. *Food Biophys.* **19**, 1134–1146. <https://doi.org/10.1007/s11483-024-09887-x> (2024).
47. Ruan, J., Li, M., Liu, Y., Ye, B. & Ling, C. Adsorption isotherm and thermodynamic properties of microwave vacuum dried tilapia fillets. *Lwt* **166**, 113766. <https://doi.org/10.1016/j.lwt.2022.113766> (2022).
48. Lim, L. T., Tang, J. & He, J. Moisture sorption characteristics of freeze dried blueberries. *J. Food Sci.* **60**, 810–814. <https://doi.org/10.1111/j.1365-2621.1995.tb06235.x> (1995).
49. Tsami, E., Krokida, M. & Drouzas, A. Effect of drying method on the sorption characteristics of model fruit powders. *J. Food Eng.* **38**, 381–392. [https://doi.org/10.1016/S0260-8774\(98\)00130-7](https://doi.org/10.1016/S0260-8774(98)00130-7) (1998).
50. McMinn, W. A. M., Al-Muhtaseb, A. H. & Magee, T. R. A. Enthalpy–entropy compensation in sorption phenomena of starch materials. *Food Res. Int.* **38**, 505–510. <https://doi.org/10.1016/j.foodres.2004.11.004> (2005).
51. de Araújo, A. L. & da Silva Pena, R. Moisture desorption behavior and thermodynamic properties of pulp and seed of Jambolan (*Syzygium cumini*). *Heliyon* **8** <https://doi.org/10.1016/j.heliyon.2022.e09443> (2022).
52. Argyropoulos, D. & Müller, J. Effect of convective-, vacuum- and freeze drying on sorption behaviour and bioactive compounds of lemon balm (*Melissa officinalis* L). *J. Appl. Res. Med. Aromatic Plants*. **1**, 59–69. <https://doi.org/10.1016/j.jarmap.2014.06.001> (2014).
53. Van den Berg, C. *Water Activity Andits Estimation in Foodsystems: Theoretical Aspects* (Academic, 1981).

Acknowledgements

This research project was supported by Chulalongkorn University, the Second Century Fund (C2F), which funded Dr. Mohamed Fikry's C2F High-Potential Postdoctoral Fellowship (2025). Additionally, the authors would like to express their appreciation to the Department of Agricultural Engineering, College of Food and Agriculture Sciences, King Saud University; the Date Palm Research Center of Excellence, King Faisal University, Saudi Arabia; and the Department of Food Technology, Faculty of Science, Chulalongkorn University, for their valuable technical support in this work.

Author contributions

Mohamed Fikry: Conceptualization, Methodology, Data analysis, Data visualization, Writing – original draft. Kitipong Assatarakul: Writing – review & editing, Writing – original draft, Supervision, Project administration, Correspondence. Saleh Al-Ghamdi: Data analysis, Data visualization, Writing – review & editing. Bandar Alfaifi: Data analysis, Data visualization, Writing – review & editing. Nashi Alqahtani: Writing – original draft, Data visualization, Writing – review & editing. Mansour N. Ibrahim: Experimentation, Data visualization, Writing – review & editing. Muhammad Umar: Experimentation, Data visualization, Writing – review & editing.

Funding

This study was funded by the Second Century Fund (C2F) fellowship of Chulalongkorn University (to Dr. Mohamed Fikry) and Department of Food Technology, Faculty of Science, Chulalongkorn University, Bangkok Thailand.

Declarations

Competing interests

The authors declare no competing interests.

Additional information

Correspondence and requests for materials should be addressed to K.A.

Reprints and permissions information is available at www.nature.com/reprints.

Publisher's note Springer Nature remains neutral with regard to jurisdictional claims in published maps and institutional affiliations.

Open Access This article is licensed under a Creative Commons Attribution-NonCommercial-NoDerivatives 4.0 International License, which permits any non-commercial use, sharing, distribution and reproduction in any medium or format, as long as you give appropriate credit to the original author(s) and the source, provide a link to the Creative Commons licence, and indicate if you modified the licensed material. You do not have permission under this licence to share adapted material derived from this article or parts of it. The images or other third party material in this article are included in the article's Creative Commons licence, unless indicated otherwise in a credit line to the material. If material is not included in the article's Creative Commons licence and your intended use is not permitted by statutory regulation or exceeds the permitted use, you will need to obtain permission directly from the copyright holder. To view a copy of this licence, visit <http://creativecommons.org/licenses/by-nc-nd/4.0/>.

© The Author(s) 2025